Published in final edited form as:

Cell Chem Biol. 2018 September 20; 25(9): 1075–1085.e4. doi:10.1016/j.chembiol.2018.05.012.

Resistance to Enediyne Antitumor Antibiotics by Sequestration

Chin-Yuan Chang[1,8], **Xiaohui Yan**[1,8], **Ivana Crnovcic**[1], **Thibault Annaval**[1], **Changsoo Chang**[2,3], **Boguslaw Nocek**[2,3], **Jeffrey D. Rudolf**[1], **Dong Yang**[1], **Hindra**[1], **Gyorgy Babnigg**[3,4], **Andrzej Joachimiak**[2,3,4], **George N. Phillips Jr.**[5], and **Ben Shen**[1,6,7,9,*]

[1]Department of Chemistry, The Scripps Research Institute, Jupiter, FL 33458, USA

[2]Structural Biology Center, Biosciences Division, Argonne National Laboratory, Argonne, IL 60439, USA

[3]Midwest Center for Structural Genomics, Biosciences Division, Argonne National Laboratory, Argonne, IL 60439, USA

[4]Center for Structural Genomics of Infectious Diseases, University of Chicago, Chicago, IL 60637, USA

[5]BioSciences at Rice and Department of Chemistry, Rice University, Houston, TX 77251, USA

[6]Department of Molecular Medicine, The Scripps Research Institute, Jupiter, FL 33458, USA

[7]Natural Products Library Initiative at The Scripps Research Institute, The Scripps Research Institute, Jupiter, FL 33458, USA

[8]These authors contributed equally

[9]Lead Contact

SUMMARY

The enediynes, microbial natural products with extraordinary cytotoxicities, have been translated into clinical drugs. Two self-resistance mechanisms are known in the enediyne producers—apoproteins for the nine-membered enediynes and self-sacrifice proteins for the ten-membered enediyne calicheamicin. Here we show that: (1) *tnmS1*, *tnmS2*, and *tnmS3* encode tiancimycin (TNM) resistance in its producer *Streptomyces* sp. CB03234, (2) *tnmS1*, *tnmS2*, and *tnmS3* homologs are found in all anthraquinone-fused enediyne producers, (3) TnmS1, TnmS2, and TnmS3 share a similar β barrel-like structure, bind TNMs with nanomolar K_D values, and confer resistance by sequestration, and (4) TnmS1, TnmS2, and TnmS3 homologs are widespread in

*Correspondence: shenb@scripps.edu.

AUTHOR CONTRIBUTIONS

B.S. conceived the project. A.J., G.N.P., and B.S. designed the experiments. C.-Y.C., X.Y., and T.A. constructed the plasmids and purified the proteins for enzyme activity assay and crystallization. C.-Y.C., C.C., B.N., and G.B. collected the diffraction data and solved the crystal structure. C.-Y.C. and J.D.R. analyzed the crystal structures. X.Y. and J.D.R. contributed to the bioinformatics analysis. X.Y., D.Y., I.C., and Hindra produced and isolated the anthraquinone-fused enediynes. C.-Y.C., X.Y., J.D.R., G.N.P., and B.S. analyzed the results. C.-Y.C., X.Y., and J.D.R wrote the manuscript with inputs from all co-authors. B.S. edited and finalized paper.

SUPPLEMENTAL INFORMATION

Supplemental Information includes six figures, three tables, and two data files and can be found with this article online at https://doi.org/10.1016/j.chembiol. 2018.05.012.

DECLARATION OF INTERESTS

B.S. has filed a patent (US, 2018/0009823 A1). The other authors declare no competing interests.

nature, including in the human microbiome. These findings unveil an unprecedented resistance mechanism for the enediynes. Mechanisms of self-resistance in producers serve as models to predict and combat future drug resistance in clinical settings. Enediyne-based chemotherapies should now consider the fact that the human microbiome harbors genes encoding enediyne resistance.

Graphical Abstract

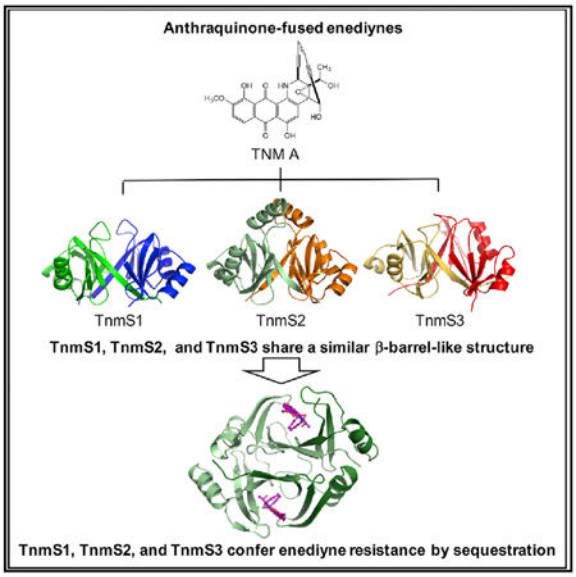

In Brief

TnmS1, TnmS2, and TnmS3 confer tiancimycin resistance by sequestration. Their homologs are found in all anthraquinone-fused enediyne producers and are widespread in nature, including in the human microbiome. These findings unveil an unprecedented resistance mechanism for the enediynes and should be considered in future efforts to develop enediyne-based chemotherapies.

INTRODUCTION

The enediynes represent one of the most fascinating families of natural products for their unprecedented molecular architecture and extraordinary cytotoxicity against a broad panel of cancer cell lines (Van Lanen and Shen, 2008). Since the determination of the enediyne chromophore structure of neocarzinostatin (NCS) in 1985 (Edo et al., 1985), 13 enediynes have been isolated and structurally characterized (Yan et al., 2016, 2017). All enediynes contain an enediyne core consisting of two acetylenic groups conjugated to a double bond or incipient double bond within a nine- or ten-membered carbocycle (Galm et al., 2005). Members of the nine-membered enediyne core subcategory include NCS, C-1027, kedarcidin, maduropeptin, and N1999A2. Members of the ten-membered enediyne core subcategory include calicheamicin (CAL), esperamicin, namenamicin, shishijimicin, and the anthraquinone-fused enediynes dynemicin (DYN), uncialamycin (UCM), tiancimycin (TNM), and yangpumicin (YPM). As a consequence of this structural feature, the enediynes share a common mode of action—electronic rearrangement of the nine- or ten-membered

enediynes core to produce a transient benzenoid diradical. When positioned within the minor groove of DNA, the diradical abstracts hydrogen atoms from the deoxyribose backbone of DNA. The DNA-centered radicals can then cause interstrand crosslinks, react with molecular oxygen leading ultimately to DNA double-strand breaks, or both, endowing the enediyne natural products with an extraordinary cytotoxicity (Kennedy et al., 2007).

The enediynes have been successfully translated into clinical drugs by targeted delivery. Poly(styrene-co-maleic acid)-conjugated NCS (SMANCS) has been marketed since 1994 for the treatment of hepatocellular carcinoma (Abe and Otsuki, 2002). A CD33 monoclonal antibody-CAL conjugate, gemtuzumab ozogamicin (Mylotarg), and a CD22 monoclonal antibody-CAL conjugate, inotuzumab ozogamicin (Besponsa), have been approved since 2000 and 2017, respectively, for the treatment of acute myeloid leukemia (Pfizer voluntarily withdrew Mylotarg from the market in 2010, and the US Food and Drug Administration reapproved Mylotarg in 2017). In addition, C-1027, also known as lidamycin (Chen et al., 2015), and UCM as payloads of antibody-drug conjugates for cancers have been actively pursued in several preclinical studies (Li et al., 2016; Shen et al., 2015).

Self-resistance mechanisms are essential for antibiotic-producing microbes to protect themselves from the lethal effects of their own cytotoxic molecules. The three major self-resistance mechanisms in antibiotic-producing bacteria are: (1) modification or degradation of the antibiotics to render them biologically inactive, (2) modification of the antibiotic targets to render them insensitive, and (3) effluxion of the antibiotics out of the cell to keep them under the lethal level (Blair et al., 2015). In addition to these common resistance mechanisms, antibiotic sequestration, target overproduction, and metabolic pathway modification are also known (Blair et al., 2015). Self-resistance determinants in the producers represent a major reservoir for the development of drug resistance in the clinical setting by horizontal gene transfer. Although direct horizontal gene transfer has only been shown in a few cases, the evidence is now clear that the environment, including antibiotic producers, is the single largest reservoir of resistance (Surette and Wright, 2017). Mechanisms of self-resistance in antibiotic producers, therefore, serve as models to predict and combat future drug resistance in clinical settings.

Two mechanisms of self-resistance are known for the enediyne producers. Members of the nine-membered enediyne core subcategory are produced as chromoproteins, employing apoproteins to stabilize the otherwise unstable enediyne chromophores and facilitate their transport (Liu and Shen, 2000). For the ten-membered enediyne core subcategory, only CAL has a reported mechanism—the self-sacrifice proteins, encoded by *calC*, *calU16*, and *calU19* in the *cal* biosynthetic gene cluster, which trigger aromatization of the enediyne core via radical-dependent protein cleavage (Biggins et al., 2003; Elshahawi et al., 2014). The anthraquinone-fused enediynes are a subclass of ten-membered enediyne core subcategory that includes DYN (Konishi et al., 1989), UCM (Davies et al., 2005), TNM (Yan et al., 2016), and YPM (Yan et al., 2017) (Figure 1A). The gene cluster for DYN biosynthesis has been cloned previously (Gao and Thor-son, 2008). We recently cloned and characterized the gene clusters for TNM (Yan et al., 2016), UCM (Yan et al., 2016), and YPM (Yan et al., 2017) biosynthesis. We subsequently constructed an enediyne genome neighborhood network (GNN), which allowed prediction of new structural features and biosynthetic

insights that could be exploited for enediyne discovery (Rudolf et al., 2016; Yan et al., 2016, 2017). However, the mechanism of self-resistance for the anthraquinone-fused enediynes remains unknown.

Here we report (1) the discovery and characterization of sequestration as an unprecedented mechanism of self-resistance for the anthraquinone-fused enediynes and (2) the wide distribution of these resistance elements in nature, including in the human microbiome. These findings should now be considered in current and future efforts to develop enediyne-based chemotherapies.

RESULTS AND DISCUSSION

Bioinformatics Analysis Revealing Candidates for the Self-Resistance Genes in the Biosynthetic Gene Clusters of Anthraquinone-Fused Enediynes

We first constructed an enediyne GNN, including all predicted and experimentally confirmed enediyne biosynthetic gene clusters, to search for candidates conferring self-resistance to the anthraquinone-fused enediynes. The GNN clearly revealed additional homologs of the apoproteins, known for the nine-membered enediyne core subcategory, and the self-sacrifice proteins, known for the ten-membered enediyne CAL, suggesting that both mechanisms are likely shared by many other enediynes; these findings also demonstrated the utility of GNN in identifying candidates conferring enediyne resistance by the known mechanisms (Figures 1C and S1). Strikingly, GNN analysis failed to identify any candidates for the two known resistance mechanisms from the gene clusters encoding the biosyn-thesis of the four anthraquinone-fused enediynes, DYN, UCM, TNM, and YPM (Figure 1A). Since these producers must have evolved self-resistance elements, close examination of the GNN revealed a distinct family of proteins, consisting of TnmS1, TnmS2, TnmS3, UcmS1, UcmS2, UcmS3, DynE14, DynE15, YpmS1, and YpmS3, from the TNM, UCM, DYN, and YPM biosynthetic machineries, that share 31%–90% amino acid sequence identities (Figures 1B, 1C, and S1; Data S1A), suggesting an unprecedented mechanism of self-resistance for the anthraquinone-fused enediynes. BLASTP analysis revealed that the proteins in this family belong to the glyoxalase super-family, which are known to perform versatile functions, varying from isomerization (Cameron et al., 1997), oxidative cleavage of C-C bonds (Cho et al., 2010), epimerization (McCarthy et al., 2001), and epoxide hydrolysis (Thompson et al., 2013). Selected members in this superfamily are also known to render antibiotics ineffective, such as fosfomycin epoxide hydrolases and thiol transferases (Fillgrove et al., 2003; Thompson et al., 2013, 2014), and bleomycin (BLM) (Dumas et al., 1994) and mitomycin (Martin et al., 2002) binding proteins. With the exception of the antibiotic binding proteins, proteins in this family often possess the conserved amino acid residues His, Glu, and Asp for metal chelating. Since TnmS1, TnmS2, TnmS3, UcmS1, UcmS2, UcmS3, DynE14, DynE15, YpmS1, and YpmS3 lacked these conserved residues, we hypothesized, in the absence of alternative proposals for these proteins to play a role in biosynthesis of the anthraquinone-fused enediynes, that they might be antibiotic binding proteins that confer DYN, UCM, TNM, and YPM resistance by sequestration.

Deletion of the *tnmS1*, *tnmS2*, and *tnmS3* Genes in *Streptomyces* sp. CB03234 Confirming their Necessity in Encoding TNM Resistance

We next decided to use *Streptomyces* sp. CB03234, the wild-type producer of TNMs, as a model to investigate the self-resistance mechanisms for the anthraquinone-fused enediynes *in vivo*, confirming that *tnmS1*, *tnmS2*, and *tnmS3* are necessary to endow *Streptomyces* sp. CB03234 with high resistance to TNMs. We deleted a 5.5-kb DNA fragment, harboring *tnmS1*, *tnmS2*, and *tnmS3*, as well as three additional genes, *tnmT1* and *tnmT2* (encoding two putative transporters) and *tnmR4* (encoding a putative regulator), which were interspersed among the three predicted resistance genes (Figure 1B), in *Streptomyces* sp. CB03234 to generate the Δ*tnmS1-tnmS3* mutant strain SB20003. Its sensitivity to TNMs was first tested by a disk diffusion assay, with the wild-type *Streptomyces* sp. CB03234 as a positive control. While CB03234 showed high resistance, SB20003 was remarkably sensitive to TNM A, and obvious inhibition zones were observed for SB20003 even at the lowest amount of TNM A (1 ng) tested (Figure 2A). We further determined the minimal inhibitory concentrations (MICs) of TNM A against CB03234 and SB20003 by a plate growth assay, with *Streptomyces lividans* TK24, a naive strain that is sensitive to TNM A, as a negative control. SB20003 was shown to be extremely sensitive to TNM A, with an MIC of 4 ng/mL, which was the same as the MIC for *S. lividans* TK24 (4 ng/mL) and was minimally 125-fold more sensitive than the MIC for CB03234 (500 ng/mL) (Table 1; Figure S2A). These results unambiguously establish that the inherent self-resistant elements for TNMs in *Streptomyces* sp. CB03234 reside within this six-gene fragment and that there are no other genes, outside the *tnm* biosynthetic gene cluster, that encode TNM resistance.

The *tnmS1*, *tnmS2*, and *tnmS3* Genes and their Homologs Encoding Self-Resistance for All Anthraquinone-Fused Enediynes, Show Cross-Resistance

We then focused on *tnmS1*, *tnmS2*, and *tnmS3* genes from the *tnm* cluster, as well as their homologs *ucmS1*, *ucmS2*, and *ucmS3* genes from the *ucm* cluster, *dynE14* and *dynE15* genes from the *dyn* cluster, and *ypmS1*and *ypmS3* genes from the *ypm* cluster for comparative studies (Figure 1), and revealed that they encoded self-resistance to the four anthraquinone-fused enediynes TNM, UCM, DYN, and YPM, respectively, capable of conferring cross-resistance. We adopted an *in vivo* approach to screen if *tnmS1*, *tnmS2*, *tnmS3*, or their homologs could confer resistance to TNMs or the other anthraquinone-fused enediynes UCM, DYN, and YPM, respectively, in *E. coli* BL21(DE3), which is known to be sensitive to these enediyne natural products. Each of the candidate-resistant genes was cloned into pET28a, affording expression plasmids pBS20007 to pBS20016, and transformed into *E. coli* BL21(DE3), yielding recombinant strains SB20004 to SB20013 (Table S2). Disk diffusion assays revealed that SB20004[C0]SB20013 are significantly more resistant to the corresponding anthraquinone-fused enediynes, in comparison with the negative control *E. coli* BL21(DE3)/pET28a (Figure 2B). These results provided direct evidence, supporting that *tnmS1*, *tnmS2*, *tnmS3*, or their homologs, individually, was sufficient to endow *E. coli* BL21(DE3) with resistance to their respective anthraquinone-fused enediynes *in vivo*. We subsequently determined the MICs of TNM A against SB20004, SB20005, and SB20006 by the plate growth assay for quantitative comparison. Expression of *tnmS1*, *tnmS2*, or *tnmS3* in*E. coli* BL21(DE3) revealed a similar level for protein overproduction (Figure S2B), and individually endowed *E. coli* BL21(DE3) with

>1,000-fold increase in cellular resistance to TNM A as exemplified by the MICs for SB20004 (2,560 ng/mL), SB20005 (2,560 ng/mL), and SB20006 (20,480 ng/mL) in comparison with the *E. coli* BL21(DE3) (2.5 ng/mL) (Table 1; Figure S2C). Furthermore, SB20004, SB20005, and SB20006 showed cross-resistance to UCM, DYN, and YPM (Figure S3A). These results support a common self-resistance mechanism for the anthraquinone-fused enediynes.

TnmS1, TnmS2, and TnmS3 Binding TNMs with Nanomolar Affinity

We subsequently characterized the TnmS1, TnmS2, and TnmS3 proteins *in vitro*, revealing that they bind TNMs with nanomolar affinity. Recombinant TnmS1, TnmS2, and TnmS3 proteins were produced in *E. coli* and purified to homogeneity. At high concentration (50 mg/mL), the purified TnmS1, TnmS2, and TnmS3 appeared light yellow. To identify the yellow pigment co-purified with TnmS1, TnmS2, and TnmS3, these proteins were denatured by treating with trifluoroacetic acid. The released yellow pigment, which was isolated and subjected to LC-MS analysis, was identified to be riboflavin in comparison with an authentic standard. Given the low occupancy (<20%) and micromolar K_D values of riboflavin to TnmS1, TnmS2, and TnmS3 (Figure S4; Table 2), we concluded that the co-purified riboflavin resulted from adventitious binding of riboflavin to these proteins upon their overproduction in *E. coli* and would not interfere with TnmS1, TnmS2, and TnmS3 binding to TNMs, thereby their ability to confer TNM resistance.

To directly measure the binding of TNMs to TnmS1, TnmS2, and TnmS3, we first removed the partially bound riboflavin from TnmS1, TnmS2, and TnmS3 by treatment with activated charcoal. TNM A and TNM C (Figure 1A) were used as representative anthraquinone-fused enediynes to measure their direct binding to TnmS1, TnmS2, and TnmS3 *in vitro*. The purified TnmS1, TnmS2, and TnmS3 were each found to be dimeric in solution upon analysis by size-exclusion chromatography (Figure S5A). Fluorescence-quenching analysis revealed that TNM A and TNM C were tightly bound by TnmS1, TnmS2, and TnmS3 with nanomolar K_D values (Figure S4; Table 2). TNM A, upon recovery from binding to TnmS1, TnmS2, and TnmS3, showed no modification or degradation, further demonstrating the non-covalent, non-destructive, and reversible binding between these proteins and TNMs.

Crystal Structures of TnmS1, TnmS2, and TnmS3 Revealing the Molecular Details for Resistance to the Anthraquinone-Fused Enediynes by Sequestration

We solved the crystal structures of TnmS1, TnmS2, and TnmS3 to understand the molecular details of TNM binding, revealing sequestration as an unprecedented self-resistance mechanism for the anthraquinone-fused enediynes. TnmS1, TnmS2, and TnmS3 are packed as homodimers in crystal structures, consistent with their oligomeric structures determined upon size-exclusion chromatography. Despite their low amino acid sequence identities, ranging from 16% to 29%, TnmS1, TnmS2, and TnmS3 were found to share similar structural folds with known antibiotic binding proteins, such as BLM (PDB: 1EWJ, 1QTO, and 1BYL) (Maruyama et al., 2001; Kawano et al., 2000; Dumas et al., 1994) and mitomycin (PDB: 1KLL) (Martin et al., 2002) (Data S1). Each monomer of TnmS1, TnmS2, and TnmS3 contains an N- and a C-terminal domain with a β-α-β-β-β topology (Figure 3A). The strand β1 in the N-terminal domain contributes to dimerization by alternate arm

exchange between the two monomers to form a β barrel-like structure and the two large concavities (Figure 3A). The amino acid sequence of TnmS2 is 9 and 11 residues longer than that of TnmS1 and TnmS3, respectively. Structural comparison of TnmS1, TnmS2, and TnmS3 revealed an α helix (α2) comprising 12 amino acids in TnmS2, instead of a loop in TnmS1 or TnmS3, which connects the N- and C-terminal domains (Figure 3A; Data S1B).

The structure of TnmS3 in complex with TNM A shows that each cavity houses one TNM A molecule (Figure 4A). TnmS3 undergoes a slight conformational change in β6-loop-β7 upon TNM A binding (Figure 4B). The loop between β6 and β7 shifts ~1.5Å upon TNM A binding, and the side chains of Trp100 and Gln103 flip into new conformations to interact with TNM A (Figure 4B). The structure of TnmS3 in complex with TNM C, a biosynthetic intermediate of TNM A accumulated by the Δ*tnmH* mutant strain *Streptomyces* sp. SB20002 (Yan et al., 2016, 2017), shows a similar binding environment as TNM A in TnmS3 (Figures 4C and 4D). The side chain at C-26 of TNM C reveals no strong interaction with TnmS3 (Figures 1A and 4D). The complex structures of TnmS3 with TNM A and TNM C, therefore, provide direct evidence and reveal the molecular details of how TnmS3 sequesters TNMs. Thus, TNMs are sequestered in the cavity of the β barrel-like structure by three main interactions (Figure 4C):(1) the flat anthraquinone moiety of TNM A is sandwiched between the side chains of $Trp100^{A}$ and $Trp42^{B}$ via electrostatic interactions of the aromatic rings; (2) the side chains of $Gln103^{A}$, $Gln7^{A}$, $His39^{B}$, and the main chain amine group of $Val38^{B}$ provide hydrogen bond interactions with the hydroxyl and epoxide groups of TNM A; and (3) $Gly70^{A}$ and $Leu72^{A}$ and $Leu8^{B}$, $Trp42^{B}$, $Trp59^{B}$, and $Phe60^{B}$ create a hydrophobic environment to accommodate the enediyne core.

By superposition of TnmS1 and TnmS2 with the structure of TnmS3 in complex with TNM A, the binding modes of TNM A in TnmS1 and TnmS2 were mapped. The models of TnmS1 and TnmS2 in complex with TNM A revealed that the cavities of the β barrel-like structures provide sufficient space to accommodate TNM A, the binding residues of which are proposed (Figure 3B): (1) the anthraquinone moiety interacts electrostatically with Trp41 and Phe104 in TnmS1 and Trp41 and Tyr114 in TnmS2, (2) the epoxide ring is hydrogen bonded by Asn108 in TnmS1 and Glu117 in TnmS2, and (3) the enediyne core interacts hydrophobically with Trp41, Val62, Phe71, and Leu120 and Leu39 in TnmS1, and Trp41, Val55, Val85, and Trp127 in TnmS2.

Taken together, both the anthraquinone moiety and the enediyne core contribute to the major interactions between the enediynes and the binding proteins, accounting for the findings that TnmS1, TnmS2, and TnmS3 can confer resistance to varying members of the TNMs and cross-resistance to other members of the anthraquinone-fused enediynes (Figures 1A and S3A). It is fascinating to note that each of the anthraquinone-fused enediyne producers harbors multiple genes encoding proteins with the same mechanism of self-resistance (Figures 1B and 1C). A similar phenomenon has been observed for the CAL producer that encodes three self-sacrifice proteins to confer CAL resistance (Big-gins et al., 2003; Elshahawi et al., 2014). Multiple resistance genes may ensure that sufficient resistance proteins are available to accommodate the extreme toxicity of the enediynes at all times during their biosynthesis. In addition to the final anthraquinone-fused enediyne natural products, biosynthetic intermediates and shunt metabolites have also been isolated from

these producers (Konishi et al., 1989; Davies et al., 2005; Gao and Thorson, 2008; Yan et al., 2016), indicative that multiple cytotoxic molecules may be accumulated during their biosynthesis. Multiple resistance genes would allow the producers to evolve proteins with varying substrate specificity to account for enediyne structural diversity during biosynthesis, a hypothesis that would be consistent with the findings that TnmS1, TnmS2, and TnmS3 bind TNM A and TNM C with varying K_D values (Table 2; Figure S4A).

We also solved the structure of TnmS3 in complex with riboflavin (Figure S5C), and mapped riboflavin binding in TnmS2 (Figure S5B), revealing that riboflavin binds TnmS2 and TnmS3 at the same cavity as TNMs. In analogy to the anthraquinone moiety of TNMs, the isoalloxazine ring of riboflavin is sandwiched between the side chains of Trp41 and Tyr 114 in TnmS2 and Trp42 and Trp100 in TnmS3 via electrostatic interactions (Figures S5B and S5C), accounting for the adventitious binding of riboflavin upon production of these proteins in *E. coli*. In contrast, despite the fact that TnmS1, TnmS2, and TnmS3 share the same overall structural folds as several antibiotic binding proteins, including the BLM and mitomycin binding proteins, they feature distinct ligand binding cavities (Figure S6) (Maruyama et al., 2001; Martin et al., 2002). This is consistent with the findings that TnmS1, TnmS2, and TnmS3 displayed no cross-resistance to BLM or mitomycin, respectively, upon overproduction in *E. coli* (Figures S3B and S3C).

Homologs of TnmS1, TnmS2, and TnmS3 from the Human Microbiome Conferring Resistance to TNM A

Homologs of TnmS1, TnmS2, and TnmS3 are widely distributed in nature, including the human microbiome, and confer resistance to anthraquinone-fused enediynes. Inspired by the unprecedented resistance mechanism to the anthraqui-none-fused enediynes, we constructed a sequence similarity network (Zhao et al., 2014) of 205,686 proteins from the glyoxalase family (InterPro family IPR029068, release 65.0, as of October 30, 2017) to search for homologs of TnmS1, TnmS2, and TnmS3 from the InterPro database. When an *e* value threshold of 10^{-20} (~30% sequence identity over 80 amino acids) was applied, 4,095 homologs of TnmS1, TnmS2, and TnmS3 were grouped in a large cluster. These homologs are from a broad range of bacteria, with Actinobacteria (~65%) and Proteobacteria (~22%) as the major sources, together with 19 proteins from the Archaea domain and one protein from the Eukarya domain (Figure 5; Data S2A). Strikingly, 89 of the 4,095 homologs are from the human micro-biome at different body sites. As the human microbiome has been reported as a reservoir of antibiotic resistance genes (Sommer et al., 2009), characterization of selected proteins from the 89 homologs will provide direct evidence whether these proteins could also confer resistance to the anthraqui-none-fused enediynes.

We selected five representative proteins from the human microbiota, HMPREF0765_3744 from *Sphingobacterium spiritivorum* ATCC 33300 (isolated from the urogenital tract), HMPREF1004_01465 from *Ralstonia* sp. 5_7_47FAA, HMPREF1015_01744 from *Bacillus smithii* 7_3_47FAA, HMPREF1211_07544 from *Streptomyces* sp. HGB0020, and CBFG_04671 from *Clostridiales* bacterium 1_7_47FAA (all isolated from the gastrointestinal tract), none of which possesses the gene clusters encoding enediyne biosynthesis (Data S2B). The five representative proteins, selected from the 89 homologs,

share 29%–48% amino acid sequence identities to TnmS1, TnmS2, and TnmS3, from the 89 homologs (Data S1A). We directly tested, by both *in vivo* and *in vitro* methods, their ability to confer resistance to TNM A as a representative of anthraquinone-fused enediynes. Thus, the genes encoding these five proteins were synthesized and cloned into pET28a, affording expression plasmids pBS20017 to pBS20021, and transformed into *E. coli* BL21(DE3), yielding recombinant strains SB20014 to SB20018 (Table S2). SDS-PAGE analysis confirmed that these strains produced similar levels of the five representative proteins (Figure S2B). Disk diffusion assay revealed that all five homologs confer some degree of resistance to TNM A (Figure 2C), with MICs, determined by the plate growth assay, ranging from 10 to 20,480 ng/mL (Table 1; Figure S2C). It is remarkable that HMPREF1211_07544 and CBFG_04671 confer TNM A resistance at the same level as the TnmS1, TnmS2, and TnmS3, displaying similar nanomolar K_D values (Table 2; Figure S4A). Like TnmS1, TnmS2, and TnmS3, these homologs conferred resistance specific to TNM A, and no cross-resistance to BLM or mitomycin was observed (Figure S3). Sequence alignment of TnmS1, TnmS2, TnmS3, with the five selected homologs from the human microbiome, revealed that the residues for electrostatic interactions are highly conserved in each of these proteins, while the residues for hydrogen bond and hydrophobic interactions are diverse (Data S1D).

Little is known how the human microbiome acquires its immense diversity of drug-resistance genes. Although the human microbiota has been suggested to acquire resistance genes from pathogens resistant to clinical antibiotics (Penders et al., 2013), we present here that the human microbiome already possesses the resistant elements to anthraquinone-fused enediynes, which have yet to be developed and used clinically. It has been recently reported that intratumor bacteria could produce enzymes that metabolize the anti-cancer drug into its inactive form, thereby influencing the efficacy of cancer chemotherapy (Geller et al., 2017). Although it is far from certain if these alleles are actual components of the human microbiome, rather than environmental contaminants, our findings raise the possibility that the human microbiome might impact the efficacy of anthraquinone-fused enediynes and should now be taken into consideration in current and future efforts to develop enediyne-based chemotherapies.

STAR+METHODS

KEY RESOURCES TABLE

REAGENT or RESOURCE	SOURCE	IDENTIFIER
Bacterial and Virus Strains		
Streptomyces lividans TK324	Hopwood et al., 1983	N/A
Micromonospora chersina ATCC53710	Gao and Thorson, 2008	N/A
Streptomyces sp. CB03234	Yan et al., 2016	N/A
Streptomyces uncialis DCA2648	Yan et al., 2016	N/A
Micromonospora yangpuensis DSM45577	Yan et al., 2017	N/A
Chemicals, Peptides, and Recombinant Proteins		
Selenomethionine	Acros	Cat#AC259960025

REAGENT or RESOURCE	SOURCE	IDENTIFIER
Bleomycin	bioWORLD	Cat#40210016-2
Mitomycin	RPI	Cat#M92010
Deposited Data		
Crystal structure of member of Glyoxalase/ bleomycin resistance protein/dioxygenase superfamily from *Sphaerobacter thermophilus* DSM 20745	Protein Data Bank	PDB: 4HC5 https://www.rcsb.org/structure/4hc5
TnmS1, TnmS2, and TnmS3 from *S.* sp. CB03234	GenBank	Accession No.: AME18020 AME18022 AME18026
UcmS1, UcmS2, and UcmS3 from *S. uncialis* DCA2648	GenBank	Accession No.: AMK92568 AMK92566 AMK92564
DynE14 and DynE15 from *M. chersina* ATCC53710	GenBank	Accession No.: WP_091316676 WP_091316667
YpmS1 and YpmS3 from *M. yangpuensis* DSM45577	GenBank	Accession No.: WP_091439392 WP_091439387
The selected five homologues of TnmS1, TnmS2, and TnmS3 from the human microbiome: HMPREF1015_01744, HMPREF0765_3744, HMPREF1004_01465, HMPREF1211_07544, and CBFG_04671	GenBank	Accession No.: WP_003353922 WP_003002659 WP_004633594 WP_016437401 WP_008724152
Oligonucleotides		
hmpref1015_01744 gene	Genewiz	N/A
hmpref0765_3744 gene	Genewiz	N/A
hmpref1004_01465 gene	Genewiz	N/A
hmpref1211_07544 gene	Genewiz	N/A
cbfg04671 gene	Genewiz	N/A
Recombinant DNA		
pBS8007	Tao et al., 2007	N/A
pBS20002	Yan et al., 2016	N/A
Software and Algorithms		
MOLREP	Vagin and Teplyakov, 2010	N/A
AutoSol	Terwilliger et al., 2009	N/A
HKL-3000	Minor et al., 2006	N/A
REFMAC	Murshudov et al., 1997	N/A

CONTACT FOR REAGENT AND RESOURCE SHARING

Further information and requests for resources and reagents should be directed to and will be fulfilled by the Lead Contact, Ben Shen (shenb@scripps.edu).

EXPERIMENTAL MODEL AND SUBJECTE DETAILS

E. coli BL21(DE3) was used for protein production. *Micromonospora chersina* ATCC53710, *Streptomyces* sp. CB03234, *Streptomyces uncialis* DCA2648, and *Micromonospora yangpuensis* DSM45577 were used for production of DYN, TNMs, UCM, and YPM, respectively. Culture conditions followed literature procedures, and references are provided in Method Details.

METHOD DETAILS

General Materials—Primers, plasmids, and strains used in this study are summarized in Tables S1 and S2.

Gene Cloning and Protein Production and Purification—The *tnmS1*, *tnmS2*, and *tnmS3* genes were amplified by PCR from the genomic DNA of the TNM producer *S.* sp. strain CB03234 using primers summarized in Table S1. The PCR products were cloned into pET28a to afford the expression plasmids pBS20007, pBS20008, and pBS20009, which were transformed into *E. coli* BL21(DE3) to yield recombinant strains SB20004, SB20005, and SB20006. The latter strains were grown at 37°C, 200 rpm in 1 L LB medium with 50 μg/mL kanamycin until it reached an OD_{600} =0.5. To produce the selenomethionyl (SeMet)-labeled TnmS2 protein, SB20005 was grown at 37°C, 200 rpm in 1 L of enriched M9 medium with 50 μg/mL kanamycin until it reached an OD_{600}=1.0. After air-cooling at 4°C for 60 min, methionine biosynthesis inhibitory amino acids (25 mg each/L of L-valine, L-isoleucine, L-leucine, L-lysine, L-threonine, L-phenylalanine) and 90 mg/L of selenomethionine were added. Protein overproduction was induced by 0.5 mM isopropyl-β-D-thiogalactoside (IPTG). The cells were incubated overnight at 18°C and were subsequently harvested and resuspended in lysis buffer (500 mM NaCl, 20 mM Tris, pH 8.0). Cells were disrupted by lysozyme treatment (1 mg/mL) and sonication, and the insoluble cellular material was removed by centrifugation. TnmS1, TnmS2 or SeMet-labeled SnmS2, and TnmS3 were purified using Ni-NTA affinity chromatography. The column was washed sequentially with 20 mL of lysis buffer and 12 mL of washing buffer (lysis buffer containing 50 mM imidazole) and eluted with 10 mL of elution buffer (lysis buffer containing 300 mM imidazole). The eluted protein was further purified by size exclusion chromatography using a Superdex 200 16/200 column under 200 mM NaCl and 50 mM Tris buffer, pH 8.0. The buffer was exchanged with 3-(N-morpholino)propanesulfonic acid (MOPS) buffer (20 mM, pH 7.0) using Amicon Ultra-15 concentrators (Millipore). Protein purity was examined by SDS-PAGE protein electrophoresis. Protein concentrations were determined from the absorbance at 280 nm using a calculated molar absorption coefficient (ε_{280} = 8,480, 18,450, and 17,990 M^{-1} cm^{-1} for TnmS1, TnmS2, and TnmS3, respectively). The concentration of TnmS1, TnmS2, and TnmS3 used for crystallization were 15, 20, and 30 mg/mL, respectively.

The *ucmS1*, *ucmS2*, and *ucmS3* genes from the UCM producer *Streptomyces uncialis* DCA2648, *dynE14* and *dynE15* genes from the DYN producer *Micromonospora chersina* ATCC53710, and *ypmS1* and *ypmS3* genes from the YPM producer *Micromonospora yangpuensis* DSM45577 were amplified by PCR from the corresponding genomic DNAs using primers summarized in Table S1. The genes encoding the five homologues of TnmS1,

TnmS2, and TnmS3, *hmpref1015_01744*, *hmpref0765_3744*, *hmpref1004_01465*, *hmpref1211_07544*, and *cbfg04671*, were synthesized with their codons optimized for *E. coli* expression (Gouy and Gautier, 1982). The targeted genes were cloned into pET28a to afford the expression plasmids pBS20010 to pBS20021, which were transformed into *E. coli* BL21(DE3) to yield recombinant strains SB20007 to SB20018. Gene expression and protein production and purification of HMPREF1015_01744, HMPREF 0765_3744, HMPREF 1004_01465, HMPREF 1211_07544, and CBFG04671 followed the same procedure described above for TnmS1, TnmS2, and TnmS3. Protein concentrations were determined from the absorbance at 280 nm using a calculated molar absorption coefficient (ε_{280} = 23,960, 12,950, 16,960, 12,490, and 22,460 M^{-1} cm^{-1} for HMPREF1015_01744, HMPREF 0765_3744, HMPREF 1004_01465, HMPREF 1211_07544, and CBFG04671, respectively).

Construction of the Δ*tnmS1–tnmS3* Mutant Strain SB20003—The Δ*tnmS1–tnmS3* mutant strain SB20003 was constructed in *S.* sp. CB03234 by gene replacement via homologous recombination. The 1.7-kb *ermE-neo* resistance cassette was amplified by PCR from pBS8007 (Tao et al., 2007) using primers tnmS1-S3tgtF and tnmS1-S3tgtR (Table S1) and used to replace the 5.5-kb *tnmS1–tnmS3* fragment in pBS20002 (Yan et al., 2016) via λ-RED-mediated PCR targeting mutagenesis (Gust et al., 2003) to generate pBS20006. The pBS20006 plasmid was then introduced into *S.* sp. CB03234 by *E. coli–Streptomyces* intergeneric conjugation, and kanamycin-resistant and apramycin-sensitive colonies were isolated and named SB20003, the genotype of which was confirmed by Southern analysis.

Production and Isolation of the Anthraquinone-Fused Enediynes TNM A, TNM C, UCM, DYN, and YPM—Production and isolation of TNM A, TNM C, UCM, DYN, and YPM from *S.* sp. CB03234, *S. uncialis* DCA2648, *M. chersina* ATCC53710, and *M. yangpuensis* DSM45577, respectively, followed literature procedures (Yan et al., 2016; Davies et al., 2005; Konishi et al., 1989). The authenticity of TNM A, TNM C, UCM, DYN, and YPM was validated by high resolution MS and ^{1}H and ^{13}C NMR analysis.

Protein Crystallization—The purified proteins were crystallized using the hanging drop vapor-diffusion method. TnmS1 was crystallized in 50 mM ammonium sulfate, 50 mM bis-Tris propane at pH 6.5, and 30% v/v pentaerythriol ethoxylate (15/4 EO/OH). SeMet-labeled TnmS2 was crystallized in 50 mM magnesium sulfate hydrate, 50 mM HEPES sodium at pH 7.0, and 1.6 M lithium sulfate monohydrate. TnmS3 was crystallized in 100 mM ammonium acetate, 100 mM bis-Tris at pH 5.5, and 17% w/v polyethylene glycol 3350. The crystals of TnmS3 in complex with riboflavin were obtained by soaking TnmS3 crystals with 1 μL of 20 μM riboflavin dissolved in the crystalized condition for 12 h. The crystals of TnmS3 in complex with TNM A or TNM C were obtained by soaking TnmS3 crystals with 0.1 μL of 5 mM TNM A or TNM C, respectively, which were dissolved in the crystalized condition with 50% DMSO, every 48 h until the color of the crystals became dark purple (~10 days).

Data Collection, Structural Determination, and Refinement—The protein crystals were transferred to a cryoprotectant solution containing glycerol (30% v/v) prior to X-ray diffraction. The diffraction data of TnmS1, TnmS2, and TnmS3 were collected at 100 K at the 19-ID beamline of the Structural Biology Center at the Advanced Photon Source,

Argonne National Laboratory (Rosenbaum et al., 2006). The data were recorded on Q315r (ADSC) for TnmS1 and TnmS3 and on Pilatus 6M (DECTRIS) for TnmS2. The diffraction data of TnmS3 complexed with TNM A or TNM C were collected at 100 K by an in-house diffraction facility equipped with Micromax-007 HEM (Rigaku). The data were recorded on Mar345dtb (Mar research). Data collection strategy, integration, and scaling were performed with the HKL3000 program package (Minor et al., 2006) for the crystals of TnmS1, TnmS2, and TnmS3 and the MOSFLM program (Vonrhein et al., 2011; Leslie, 2006) for the crystals of TnmS3 in complex with TNM A or TNM C.

The crystal structures of TnmS1 and TnmS3 were determined by the molecular replacement method of MOLREP (CCP4) (Vagin and Teplyakov, 2010) using the structure of a glyoxalase superfamily protein (PDB entry: 4HC5) as a search model. The crystal structures of TnmS3 complexed with TNM A, TNM C, or riboflavin were determined using the structure of TnmS3 as a search model. The crystal structure of TnmS2 was determined by the multi-wavelength anomalous dispersion (MAD) method. AutoSol (PHENIX) (Terwilliger et al., 2009) was used to find the phase solution and build the initial model. Extensive manual model building was performed using COOT (Emsley and Cowtan, 2004). The models were refined with REFMAC (Murshudov et al., 1997). The atomic coordinates and structure factors have been deposited in the Protein Data Bank with the accession code 5UMQ for TnmS1, 5UMW for TnmS2, 5UMP for TnmS3, and 5UMY, 6BBX, and 5UMX for TnmS3 in complex with TNM A, TNM C, and riboflavin, respectively. A summary of the crystallographic data and the refinement statistics are given in Table S3

Disk Diffusion Assay—For *S.* sp. CB03234, SB20003, and *S. lividans* TK24, disk diffusion assay was carried out using 10^5 spores for each strain in molten tryptic soy agar. Spores of the *Streptomyces* strains were mixed well with molten tryptic soy agar and poured into Petri dishes. The 7 mm disks (Whatman) were placed onto the agar and loaded with varying quantities of TNM A, ranging from 0 to 100 ng in 10 μL DMSO (Figure 2A). The inhibition zones were observed after 48 h at 28°C. For recombinant *E. coli* strains SB20004 to SB20018, as well as *E. coli* BL21(DE3)/pET-28a as a negative control, disk diffusion assays were carried out using overnight cultures diluted to OD_{600} = 0.2 in molten LB agar with 50 μg/mL kanamycin and 200 μM IPTG. The resultant *E. coli* cultures, kanamycin, and IPTG were mixed well with molten LB agar and poured into Petri dishes. The 7 mm disks (Whatman) were placed onto the agar and loaded with varying quantities of TNM A, UCM, DYN, YPM, ranging from 0 to 10 μg, BLM, ranging from 0 to 30 μg, and mitomycin, ranging from 0 to 5 μg, all in 10 μL DMSO (Figures 2B, 2C, and S3). The inhibition zones were observed after 24 h at 37°C.

Determination of MICs—For *S.* sp. CB03234, SB20003, and *S. lividans* TK24, 10^4 spores of each strain were added into 96 wells, each containing 200 μL TSB, and treated with varying concentrations of TNM A, ranging from 2.56×10^{-4} ng/mL to 2,500 ng/mL. The 96-well plates were incubated for 48 h at 28°C. For *E. coli* strains SB20004 to SB20006 and SB20014 to SB20018, as well as *E. coli* BL21(DE3)/pET-28a as a negative control, they were grown overnight at 37°C in LB medium with 50 μg/mL kanamycin. Each of the overnight cultures was then diluted to OD_{600} = 0.1 aliquot in 96 wells and was subsequently

treated with 200 mM IPTG and varying concentrations of TNM A, ranging from 0.625 ng/mL–40,960 ng/mL. The 96-well plates were incubated for 24 h at 37°C (Figures S1A and S2C).

Production of TnmS1, TnmS2, TnmS3, and their homologues in *E. coli* was examined to confirm that varying values of MICs were not due to varying expression levels. Strains SB20004-SB20006 and SB20014-SB20018, as well as BL21(DE3)/pET-28a as a negative control, were grown overnight at 37°C in LB medium with 50 μg/mL kanamycin. Each of the overnight cultures was then added to 5 mL of LB to reach OD_{600} = 0.1, induced with 200 μM IPTG, incubated for 16 h at 37°C, and harvested by centrifugation at 4000 × g for 15 min at 4°C. The pellets were resuspended in 500 μL of 50 mM Tris, pH 8.0, containing 100 mM NaCl. The cells were lysed by sonication, the cells debris were removed by centrifugation at 15,000 × g for 15 min at 4°C, and 10 μL of the supernatant were finally subjected to SDS-PAGE analysis (Figure S2B).

Measurement of Dissociation Constants of K_Ds—Dissociation constant K_Ds were determined according to literature procedure using fluorescence-quenching analysis (Sugiyama et al., 2002). Adventitiously bound riboflavin was first removed from TnmS1, TnmS2, and TnmS3 by treatment with activated charcoal. Proteins and ligands (i.e., TNM A, TNM C, or riboflavin) were mixed in 96-well plates, and the fluorescence intensity was recorded at 28°C on an Infinite M1000pro Microplate Reader (Tecan) under the condition of λ excitation = 280 nm, λ emission = 340 nm, 50 number of flashes, 20 μs integration time, and the slit-width = 5 nm. The proteins were diluted with MOPS buffer (20 mM, pH 7.0) to a final concentration of 2 μM for 180 μL in each 96-well. TNM A, TNM C, or riboflavin, with varying concentrations in 20 μL of DMSO, was then added to the protein solution. The fluorescent intensity of the resultant protein solutions was progressively quenched by the increasing concentrations of TNM A, TNM C, or riboflavin. All reactions were carried out in triplicate.

Recovery of TNM A from Its TnmS1, TnmS2, and TnmS3 Complexes—To form the protein-TNM A complexes, 2 μL of TNM A (2 mM in methanol) was mixed with 98 μL of TnmS1, TnmS2, or TnmS3 (1 mM in 20 mM MOPS buffer, pH 7.0), respectively, and incubated at room temperature for 10 min. The resultant protein-TNM A complexes were concentrated with Microcon-3 kDa centrifugal filter (Sigma-Aldrich), washed three times with 100 μL of MOPS buffer (20 mM, pH 7.0), and recovered by dissolving in 100 μL of MOPS buffer (20 mM, pH 7.0). TNM A was recovered by extracting the protein-TNM A complexes three times with equal volume of ethyl acetate. The ethyl acetate extracts were combined, dried in vacuo, and the residues were dissolved in 100 μL methanol and subjected to LC-MS analysis. The identity and integrity of TNM A recovered was confirmed by comparison with an authentic TNM A standard, and the percentage of recovered TNM A from each of the complexes was >90%.

QUANTIFICATION AND STATISTICAL ANALYSIS

For disk diffusion assay and MICs determination, each sample was repeated two times. For binding assay, three independent assays of each sample were run. X-ray data collected were from single crystals.

DATA AND SOFTWARE AVAILABILITY

The crystal structures have been deposited in Protein Data Bank (http://www.rcsb.org/pdb) under ID codes 5UMQ, 5UMW, 5UMP, 5UMX, 5UMY, and 6BBX for TnmS1, TnmS2, TnmS3, TnmS3–RBF, TnmS3–TNM A, and TnmS3–TNM C, respectively.

Supplementary Material

Refer to Web version on PubMed Central for supplementary material.

ACKNOWLEDGMENTS

This work is supported in part by NIH grants GM098248, GM109456, GM121060 (to G.N.P.), GM094585 (to A.J.), CA078747, GM115575, and CA204484 (to B.S.). The use of Structural Biology Center beamlines at the Advanced Photon Source was supported in part by the U.S. Department of Energy, Office of Biological and Environmental Research, grant DE-AC02–06CH11357 (to M.E.C. and A.J.). We thank the John Innes Center, Norwich, UK, for providing the REDIRECT technology kit. C.-Y.C., I.C., and J.D.R. are supported in part by postdoctoral fellowships from the Academia Sinica – The Scripps Research Institute Talent Development Program, the German Research Foundation, and the Arnold and Mabel Beckman Foundation, respectively. This is manuscript no. 29647 from The Scripps Research Institute.

REFERENCES

Abe S, and Otsuki M (2002). Styrene maleic acid neocarzinostatin treatment for hepatocellular carcinoma. Curr. Med. Chem. Anticancer Agents 2, 715–726. [PubMed: 12678722]

Biggins JB, Onwueme KC, and Thorson JS (2003). Resistance to enediyne antitumor antibiotics by CalC self-sacrifice. Science 301, 1537–1541. [PubMed: 12970566]

Blair JMA, Webber MA, Baylay AJ, Ogbolu DO, and Piddock LJV (2015). Molecular mechanisms of antibiotic resistance. Nat. Rev. Microbiol 13, 42–51. [PubMed: 25435309]

Cameron AD, Olin B, Ridderstrom M, Mannervik B, and Jones TA (1997). Crystal structure of human glyoxalase I-evidence for gene duplication and 3D domain swapping. EMBO J 16, 3386–3395. [PubMed: 9218781]

Chen Y, Yu D, Zhang C, Shang B, He H, Chen J, Zhang H, Zhao W, Wang Z, Xu X, et al. (2015). Lidamycin inhibits tumor initiating cells of hepatocellular carcinoma Huh7 through GSK3b/b-catenin pathway. Mol. Carcinog 54, 1–8. [PubMed: 23857500]

Cho HJ, Kim K, Sohn SY, Cho HY, Kim KJ, Kim MH, Kim D, Kim E, and Kang BS (2010). Substrate binding mechanism of a type I extradiol dioxygenase. J. Biol. Chem 285, 34643–34652. [PubMed: 20810655]

Davies J, Wang H, Taylor T, Warabi K, Huang XH, and Andersen RJ (2005). Uncialamycin, a new enediyne antibiotic. Org. Lett 7, 5233–5236. [PubMed: 16268546]

Dumas P, Bergdoll M, Cagnon C, and Masson JM (1994). Crystal structure and site-directed mutagenesis of a bleomycin resistance protein and their significance for drug sequestering. EMBO J 13, 2483–2492. [PubMed: 7516875]

Edo K, Mizugaki M, Koide Y, Seto H, Furihata K, Otake N, and Ishida N (1985). The structure of neocarzinostatin chromophore possessing a novel bicyclo-[7,3,0]dodecadiyne system. Tetrahedron Lett 26, 331–334.

Elshahawi SI, Ramelot TA, Seetharaman J, Chen J, Singh S, Yang Y, Pederson K, Kharel MK, Xiao R, Lew S, et al. (2014). Structure-guided functional characterization of enediyne self-sacrifice resistance proteins, CalU16 and CalU19. ACS Chem. Biol 9, 2347–2358. [PubMed: 25079510]

Emsley P, and Cowtan K (2004). Coot: model-building tools for molecular graphics. Acta Crystallogr. D Biol. Crystallogr 60, 2126–2132. [PubMed: 15572765]

Fillgrove KL, Pakhomova S, Newcomer ME, and Armstrong RN (2003). Mechanistic diversity of fosfomycin resistance in pathogenic microorganisms.J. Am. Chem. Soc 125, 15730–15731. [PubMed: 14677948]

Galm U, Hager MH, Van Lanen SG, Ju J, Thorson JS, and Shen B (2005). Antitumor antibiotics: bleomycin, enediynes, and mitomycin. Chem. Rev 105, 739–758. [PubMed: 15700963]

Gao Q, and Thorson JS (2008). The biosynthetic genes encoding for the production of the dynemicin enediyne core in *Micromonospora chersina* ATCC53710. FEMS Microbiol. Lett 282, 105–114. [PubMed: 18328078]

Geller LT, Barzily-Rokni M, Danino T, Jonas OH, Shental N, Nejman D, Gavert N, Zwang Y, Cooper ZA, Shee K, et al. (2017). Potential role of intratumor bacteria in mediating tumor resistance to the chemotherapeutic drug gemcitabine. Science 357, 1156–1160. [PubMed: 28912244]

Gerlt JA, Bouvier JT, Davidson DB, Imker HJ, Sadkhin B, Slater DR, and Whalen KL (2015). Enzyme Function Initiative-Enzyme Similarity Tool (EFI-EST): a web tool for generating protein sequence similarity networks. Biochim. Biophys. Acta 1854, 1019–1037. [PubMed: 25900361]

Gouy M, and Gautier C (1982). Codon usage in bacteria: correlation with gene expressivity. Nucleic Acids Res 10, 7055–7074. [PubMed: 6760125]

Gust B, Challis GL, Fowler K, Kieser T, and Chater KF (2003). PCR-targeted *Streptomyces* gene replacement identifies a protein domain needed for biosynthesis of the sesquiterpene soil odor geosmin. Proc. Natl. Acad. Sci. USA 100, 1541–1546. [PubMed: 12563033]

Hopwood DA, Kieser T, Wright H, and Bibb MJ (1983). Plasmids, recombination and chromosome mapping in *Streptomyces lividans* 66. J. Gen. Microbiol 129, 2257–2269. [PubMed: 6631413]

Kawano Y, Kumagai T, Muta K, Matoba Y, Davies J, and Sugiyama M (2000). The 1.5Å crystal structure of a bleomycin resistance determinant from belomycin-producing *Streptomyces verticillus*. J. Mol. Biol 28, 915–925.

Kennedy DR, Ju J, Shen B, and Beerman TA (2007). Designer enediynes generate DNA breaks interstrand cross-links, or both, with concomitant changes in the regulation of DNA damage responses. Proc. Natl. Acad. Sci. USA 104, 17632–17637. [PubMed: 17978180]

Konishi M, Ohkuma H, Matsumoto K, Tsuno T, Kamei H, Miyaki T, Oki T, Kawaguchi H, VanDuyne GD, and Clardy J (1989). Dynemicin A, a novel antibiotic with the anthraquinone and 1,5-diyn-3-ene subunit. J. Antibiot. (Tokyo) 42, 1449–1452. [PubMed: 2793600]

Leslie AG (2006). The integration of macromolecular diffraction data. Acta Crystallogr. D Biol. Crystallogr 62, 48–57. [PubMed: 16369093]

Li W, Li X, Huang T, Teng Q, Crnovcic I, Rader C, and Shen B (2016). Engineered production of cancer targeting peptide (CTP)-containing C-1027 in Streptomyces globisporus and biological evaluation. Bioorg. Med. Chem 24, 3887–3892. [PubMed: 27094150]

Liu W, and Shen B (2000). Genes for production of the enediyne antitumor antibiotic C-1027 in *Streptomyces globisporus* are clustered with the cagA gene that encodes the C-1027 apoprotein. Antimicrob. Agents Chemother 44, 382–392. [PubMed: 10639366]

Martin TW, Dauter Z, Devedjiev Y, Sheffield P, Jelen F, He M, Sherman DH, Otlewski K, Derewenda ZS, and Derewenda U (2002). Molecular basis of mitomycin C resistance in Streptomyces: structure and function of the MRD protein. Structure 10, 933–942. [PubMed: 12121648]

Maruyama M, Kumagai T, Matoba Y, Hayashida M, Fujii T, Hata Y, and Sugiyama M (2001). Crystal structures of the transposon Tn5-carried bleomycin resistance determinant uncomplexed and complexed with bleomycin.J. Biol. Chem 276, 9992–9999. [PubMed: 11134052]

McCarthy AA, Baker HM, Shewry SC, Patchett ML, and Baker EN (2001). Crystal structure of methylmalonyl-coenzyme A epimerase from*P. shermanii*: a novel enzymatic function on an ancient metal binding scaffold. Structure 9, 637–646. [PubMed: 11470438]

Minor W, Cymborowski M, Otwinowski Z, and Chruszcz M (2006). HKL-3000: the integration of data reduction and structure solution – from diffraction images to an initial model in minutes. Acta Crystallogr. D Biol. Crystallogr 62, 859–866. [PubMed: 16855301]

Murshudov GN, Vagin AA, and Dodson EJ (1997). Refinement of macro-molecular structures by the maximum-likelihood method. Acta Crystallogr. D Biol. Crystallogr 53, 240–255. [PubMed: 15299926]

Penders J, Stobberingh EE, Savelkoul PHM, and Wolffs PFG (2013). The human microbiome as a reservoir of antimicrobial resistance. Front. Microbiol 4, 87. [PubMed: 23616784]

Rosenbaum G, Alkire RW, Evans G, Rotella FJ, Lazarski K, Zhang RG, Ginell SL, Duke N, Naday I, Lazarz J, et al. (2006). The Structural Biology Center 19ID undulator beamline: facility specifications and protein crystallographic results. J. Synchrotron Radiat 13, 30–45. [PubMed: 16371706]

Rudolf JD, Yan X, and Shen B (2016). Genome neighborhood network reveals insights into enediyne biosynthesis and facilitates prediction and priori-tization for discovery. J. Ind. Microbiol. Biotechnol 43, 261–276. [PubMed: 26318027]

Shen B, Hindra, Yan X, Huang T, Ge H, Yang D, Tang D, Rudolf JD, and Lohman JR (2015). Enediyne: exploration of microbial genomics to discover new anticancer drug leads. Bioorg. Med. Chem. Lett 25, 9–15. [PubMed: 25434000]

Sommer MOA, Dantas G, and Church GM (2009). Functional characterization of the antibiotic resistance reservoir in the human microflora. Science 325, 1128–1131. [PubMed: 19713526]

Sugiyama M, Kumagai T, Hayashida M, Maruyama M, and Matoba Y (2002). The 1.6-A crystal structure of the copper(II)-bound bleomycin complexed with the bleomycin-binding protein from bleomycin-producing Streptomyces verticillus. J. Biol. Chem 277, 2311–2320. [PubMed: 11706014]

Surette MD, and Wright GD (2017). Lessons from the environmental antibiotic resistome. Annu. Rev. Microbiol 71, 309–329. [PubMed: 28657887]

Tao M, Wang L, Wendt-Pienkowski E, George NP, Galm U, Zhang G, Coughlin JM, and Shen B (2007). The tallysomycin biosynthetic gene cluster from Streptoalloteichus hindustanus E465–94 ATCC 31158 unveiling new insights into the biosynthesis of the bleomycin family of antitumor antibiotics. Mol. Biosyst 3, 60–74. [PubMed: 17216057]

Terwilliger TC, Adams PD, Read RJ, McCoy AJ, Moriarty NW, Grosse-Kunstleve RW, Afonine PV, Zwart PH, and Hung LW (2009). Decision-making in structure solution using Bayesian estimates of map quality: the PHENIX AutoSol wizard. Acta Crystallogr. D Biol. Crystallogr 65, 582–601. [PubMed: 19465773]

Thompson MK, Keithly ME, Goodman MC, Hammer ND, Cook PD, Jagessar KL, Harp J, Skaar EP, and Armstrong RN (2014). Structure and function of the genomically encoded fosfomycin resistance enzyme, FosB, from Staphylococcus aureus. Biochemistry 53, 755–765. [PubMed: 24447055]

Thompson MK, Keithly ME, Harp J, Cook PD, Jagessar KL, Sulikowski GA, and Armstrong RN (2013). Structural and chemical aspects of resistance to the antibiotic fosfomycin conferred by FosB from *Bacillus cereus*. Biochemistry 52, 7350–7362. [PubMed: 24004181]

Vagin A, and Teplyakov A (2010). Molecular replacement with MOLREP. Acta Crystallogr. D Biol. Crystallogr 66, 22–25. [PubMed: 20057045]

Van Lanen SG, and Shen B (2008). Biosynthesis of enediyne antitumor antibiotics. Curr. Top. Med. Chem 8, 448–459. [PubMed: 18397168]

Vonrhein C, Flensburg C, Keller P, Sharff A, Smart O, Paciorek W, Womack T, and Bricogne G (2011). Data processing and analysis with the autoPROC toolbox. Acta Crystallogr. D Biol. Crystallogr 67, 293–302. [PubMed: 21460447]

Yan X, Chen JJ, Adhikari A, Yang D, Crnovcic I, Wang N, Chang CY, Rader C, and Shen B (2017). Genome mining of *Micromonospora yangpuensis* DSM 45577 as a producer of an anthraquinone-fused enediyne. Org. Lett 19, 6192–6195. [PubMed: 29086572]

Yan X, Ge H, Huang T, Hindra, Yang D, Teng Q, Crnovcic I, Li X, Rudolf JD, Lohman JR, et al. (2016). Strain prioritization and genome mining for enediyne natural products. MBio 7, e02104–e02116. [PubMed: 27999165]

Zhao S, Sakai A, Zhang X, Vetting MW, Kumar R, Hillerich B, San Francisco B, Solbiati J, Steves A, Brown S, et al. (2014). Prediction and characterization of enzymatic activities guided by sequence similarity and genome neighborhood networks. Elife 3, e03275.

Highlights

- The tnmS1, tnmS2, and tnmS3 genes encode tiancimycin resistance in its producer
- Their homologs are found in all anthraquinone-fused enediyne producers
- TnmS1, TnmS2, and TnmS3 bind tiancimycins, conferring resistance by sequestration
- TnmS1, TnmS2, and TnmS3 homologs are widespread, including in the human microbiome

SIGNIFICANCE

The enediynes represent one of the most fascinating families of natural products for their unprecedented molecular architecture and extraordinary cytotoxicity and have been successfully translated into clinical drugs. Two self-resistance mechanisms are known for the enediyne producers—apoproteins for the nine-membered enediynes and self-sacrifice proteins for the ten-membered enediyne calicheamicin. Here we unveil an unprecedented resistance mechanism for the enediynes by sequestration. We show that *tnmS1*, *tnmS2*, and *tnmS3* encode tiancimycin resistance in its producer, and that their homologs are found in all known anthraquinone-fused enediyne producers. TnmS1, TnmS2, and TnmS3 share a similar β barrel-like structure, bind tiancimycins with nano-molar K_D values, and confer resistance by a common mechanism. TnmS1, TnmS2, and TnmS3 homologs are widespread in nature, including the human microbiome. Mechanisms of self-resistance in producers serve as models to predict and combat future drug resistance in clinical settings. Little is known how the human microbiome acquires its immense diversity of drug-resistance genes. Although the human micro-biota has been suggested to acquire resistance genes from pathogens resistant to clinical antibiotics, we present here that the human microbiome already possesses the resistant elements to anthraquinone-fused enediynes, which have yet to be developed and used clinically. While it is far from certain if these alleles are actual components of the human micro-biome, rather than environmental contaminants, our findings raise the possibility that the human microbiome might impact the efficacy of anthraquinone-fused enediynes and should now be taken into consideration in current and future efforts to develop enediyne-based chemotherapies.

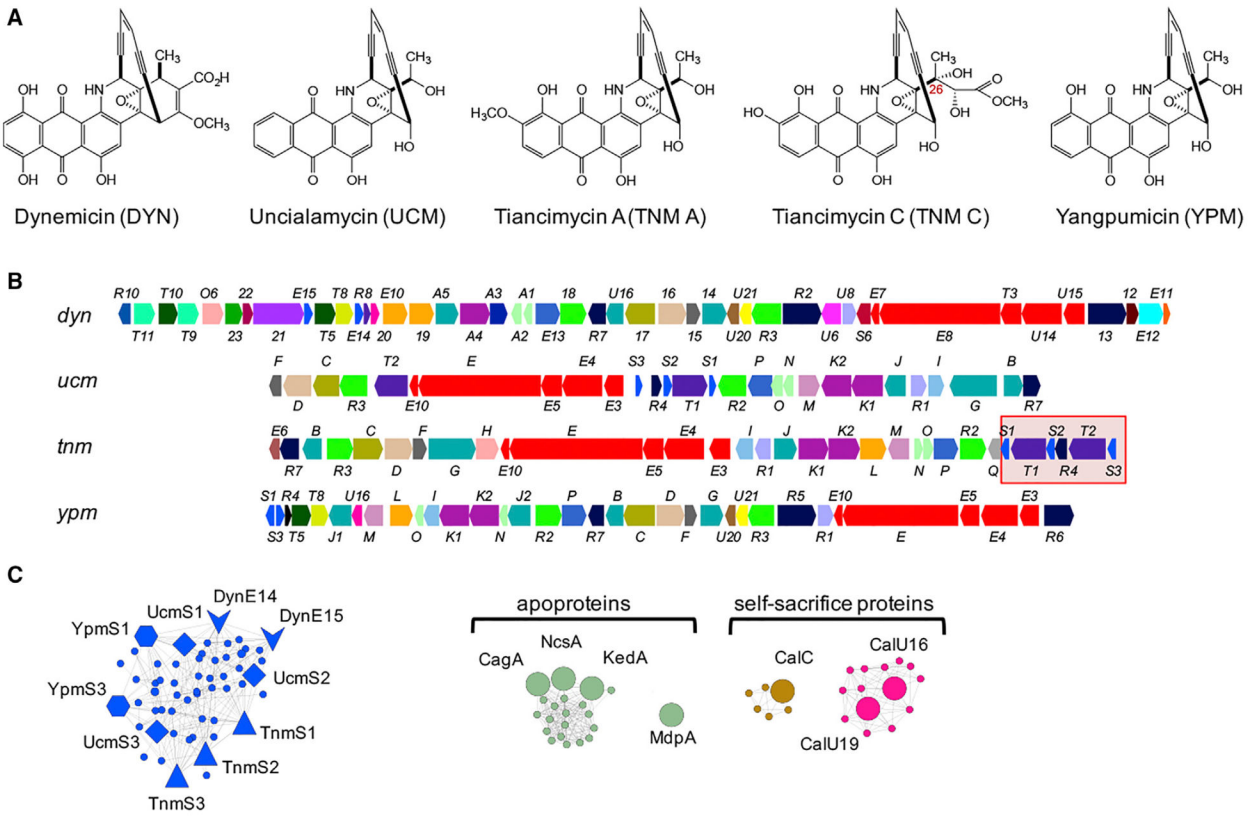

Figure 1. Bioinformatics Analysis Revealing Candidates for Self-Resistance Genes in the Biosynthetic Gene Clusters of Anthraquinone-Fused Enediynes

(A) Structures of representative anthraquinone-fused enediynes DYN, UCM, TNM A and TNM C, and YPM.

(B) The biosynthetic gene clusters of DYN, UCM, TNM, and YPM. Genes are color-coded based on GNN annotation (see Figure S1 for details). The 5.5-kb fragment harboring *tnmS1* to *tnmS3* in the *tnm* biosynthetic gene cluster is highlighted by a red box.

(C) Selected clusters from the enediyne GNN (Figure S1) that highlight apoproteins and self-sacrifice proteins conferring enediyne resistance by the two known mechanisms and reveal new candidates conferring resistance to anthraquinone-fused enediynes by an unprecedented mechanism. The genes in the same color are homologous proteins.

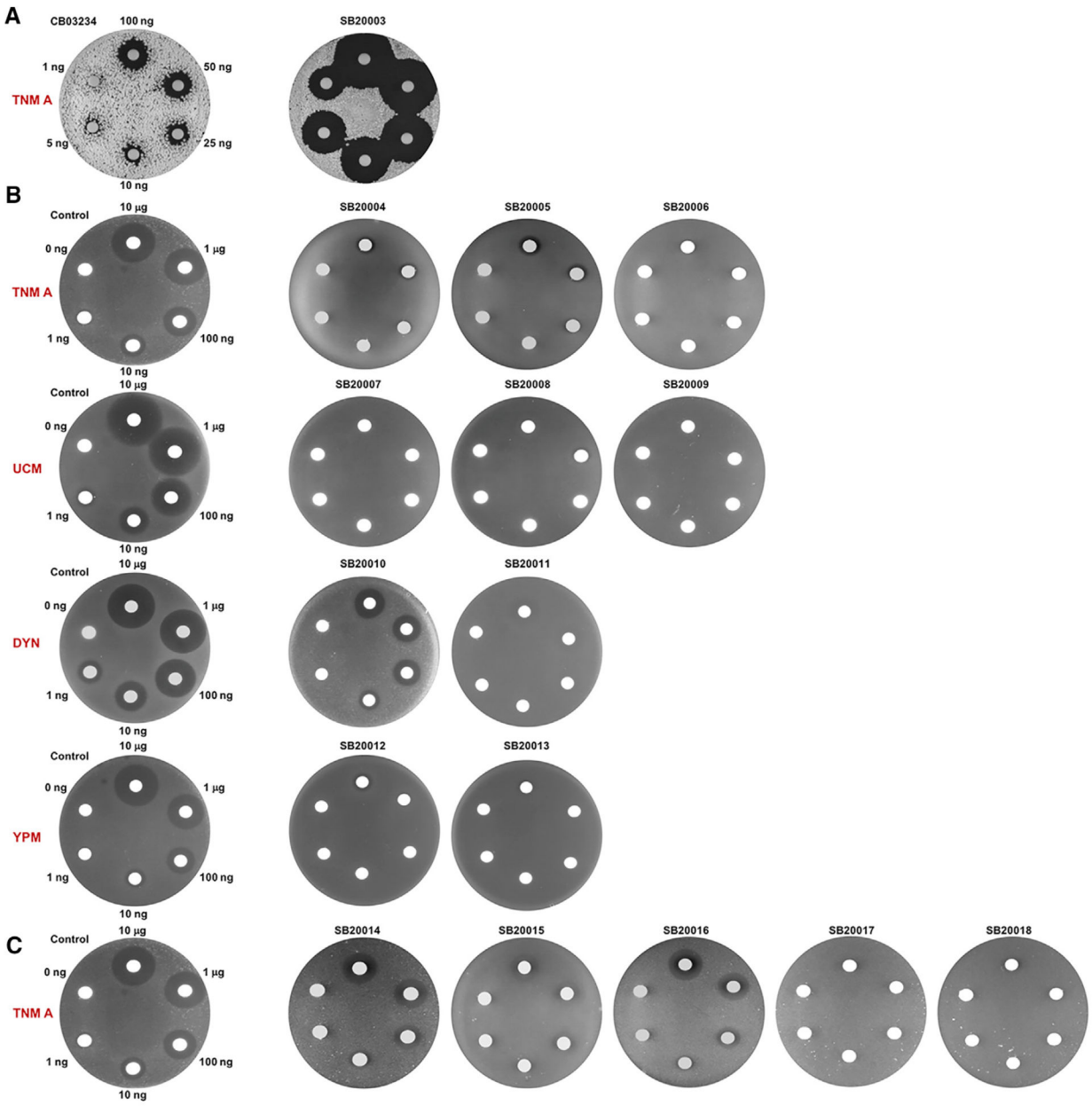

Figure 2. The *tnmS1, tnmS2, tnmS3* Genes, and their Homologs Encoding Resistance to Anthraquinone-Fused Enediynes as Demonstrated by the Disk Diffusion Assays

(A) The Δ*tnmS1-tnmS3* mutant strain SB20003 is sensitive to TNM A, in comparison with the wild-type strain CB03234 as a positive control, establishing that TnmS1, TnmS2, and TnmS3 are necessary and sufficient to confer TNM resistance in its producer.

(B) *E. coli* recombinant strains SB20004 to SB20013, expressing *tnmS1*, *tnmS2*, *tnmS3*, and their homologs from the UCM, DYN, and YPM producers, are resistant to TNM A, UCM, DYN, and YPM, respectively, in comparison with *E. coli* BL21(DE3)/pET28a as a negative control, demonstrating that each of these gene products is sufficient to confer resistance to anthraquinone-fused enediynes in their respective producers.

(C) *E. coli* recombinant strains SB20015 to SB20018, expressing the five homologs from the human microbiome, show resistance to TNM A, in comparison with *E. coli* BL21(DE3)/pET28a as a negative control, revealing that the human microbiome might already possess resistant elements to anthraquinone-fused enediynes. Depicted next to the disks are the amounts of DYN, UCM, TNM A, and YMP, respectively, loaded to each set of the diffusion assays.

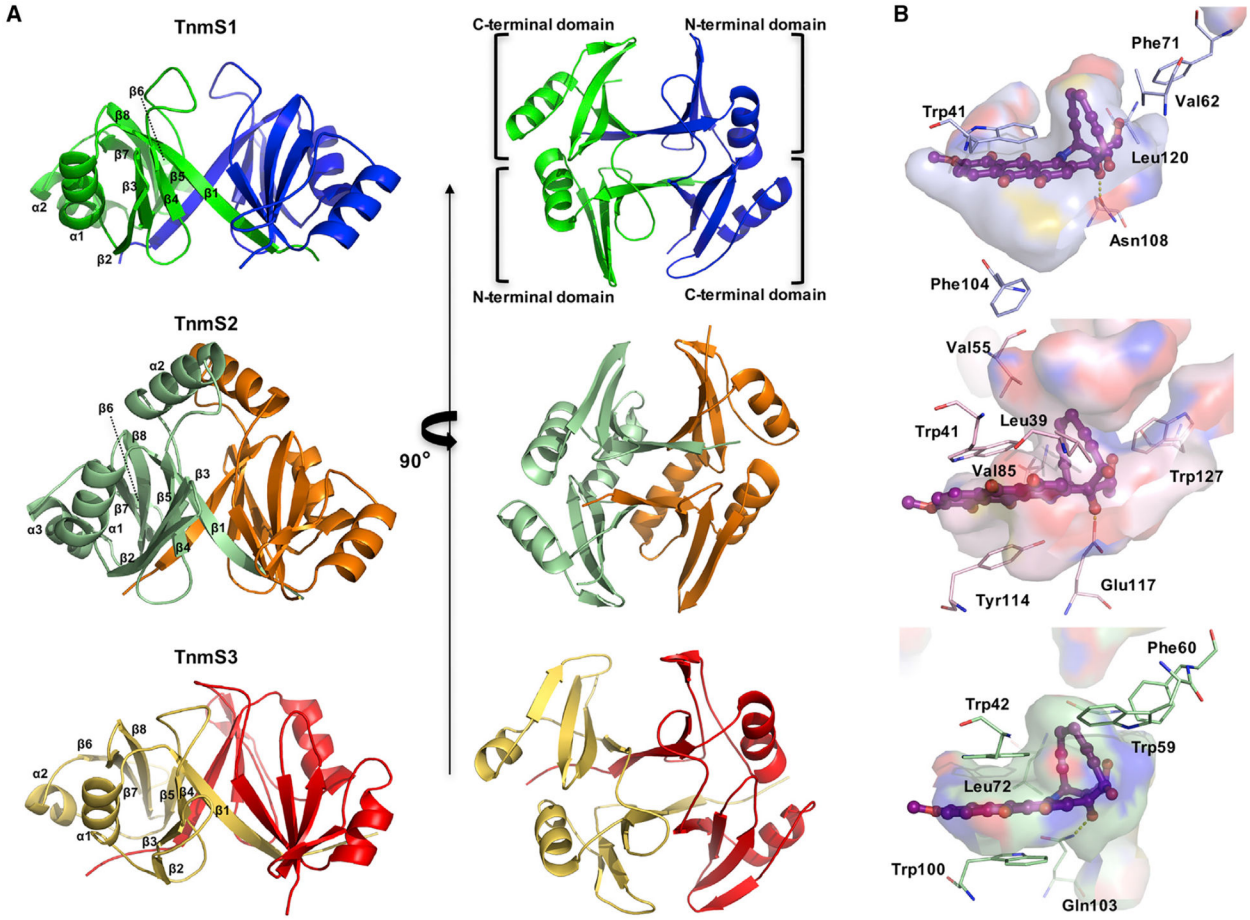

Figure 3. The Crystal Structures of TnmS1, TnmS2, and TnmS3 Revealing a β Barrel-like Structure that Forms Two Large Concavities to Accommodate TNMs

(A) The overall structures of TnmS1, TnmS2, and TnmS3 shown in ribbon diagram. The two chains of TnmS1, TnmS2, and TnmS3 are shown by green/blue, pale green/orange, and yellow/red, respectively.

(B) Solvent accessible surfaces of the binding cavities of TnmS1, TnmS2, and TnmS3, highlighting a common mode for enediyne binding. The binding modes of TNM A in TnmS1 and TnmS2 were modeled based on the structure of TnmS3 in complex with TNM A.

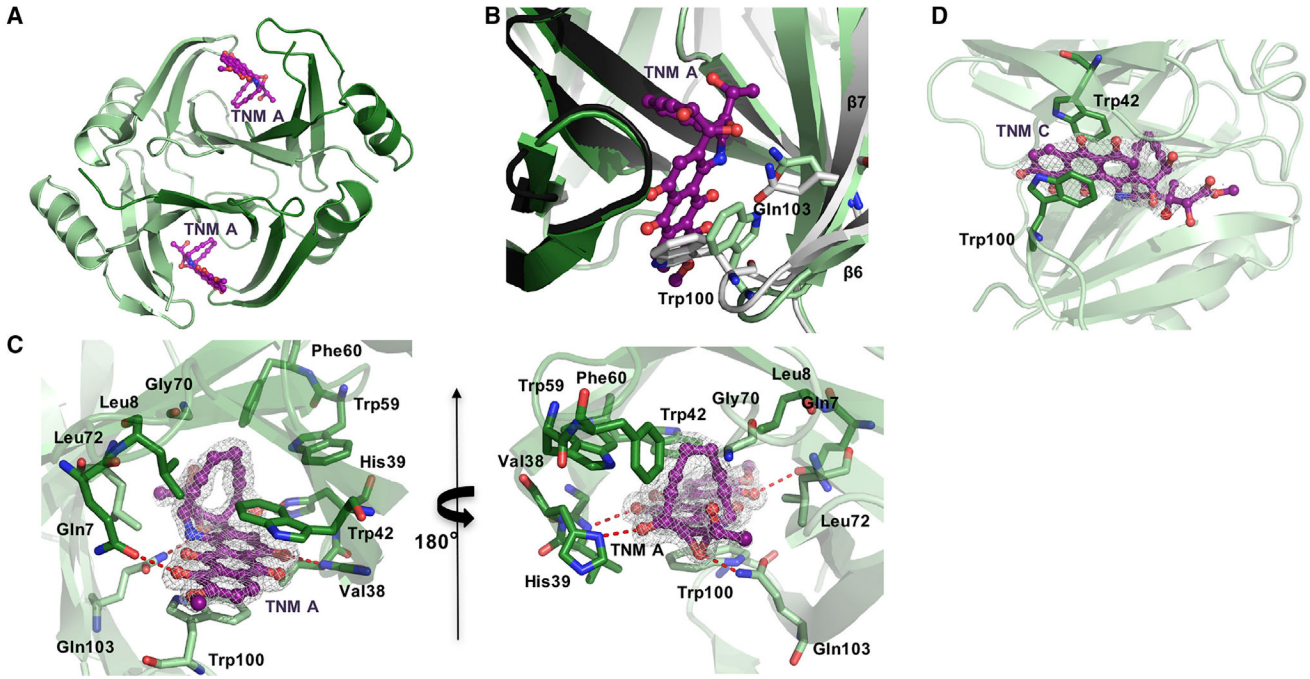

Figure 4. The Crystal Structure of TnmS3 in Complex with TNMs Revealing the Molecular Details for Resistance to the Anthraquinone-Fused Enediynes by Sequestration

(A) The overall structure of TnmS3 in complex with TNM A shown in ribbon diagram. Two molecules of TNM A are bound by one TnmS3 dimer.

(B) Local view showing that TnmS3 undergoes a slight conformational change upon TNM A binding, as depicted by the side chains of Trp100 and Gln103 flipping into new conformations to interact with TNM A, with the apo-TnmS3 structure shown in gray.

(C) Local view of the enediyne binding cavity highlighting the residues involved in interactions between TnmS3 and TNM A. Hydrogen bonds are shown in red dashed lines.

(D) The local view of the enediyne binding cavity highlighting the residues involved in interactions between TnmS3 and TNM C. While TNM A and TNM C share many of the same interactions with TnmS3, the side chain at C-26 of TNM C reveals no major interaction. The $2F_o–F_c$ electron density maps are contoured at 1s shown as white mesh. The σ-A-weighted difference ($mF_o–DF_c$) omit maps of TnmS3 in complex with TNM A and TNM C, respectively, are shown in Figure S5.

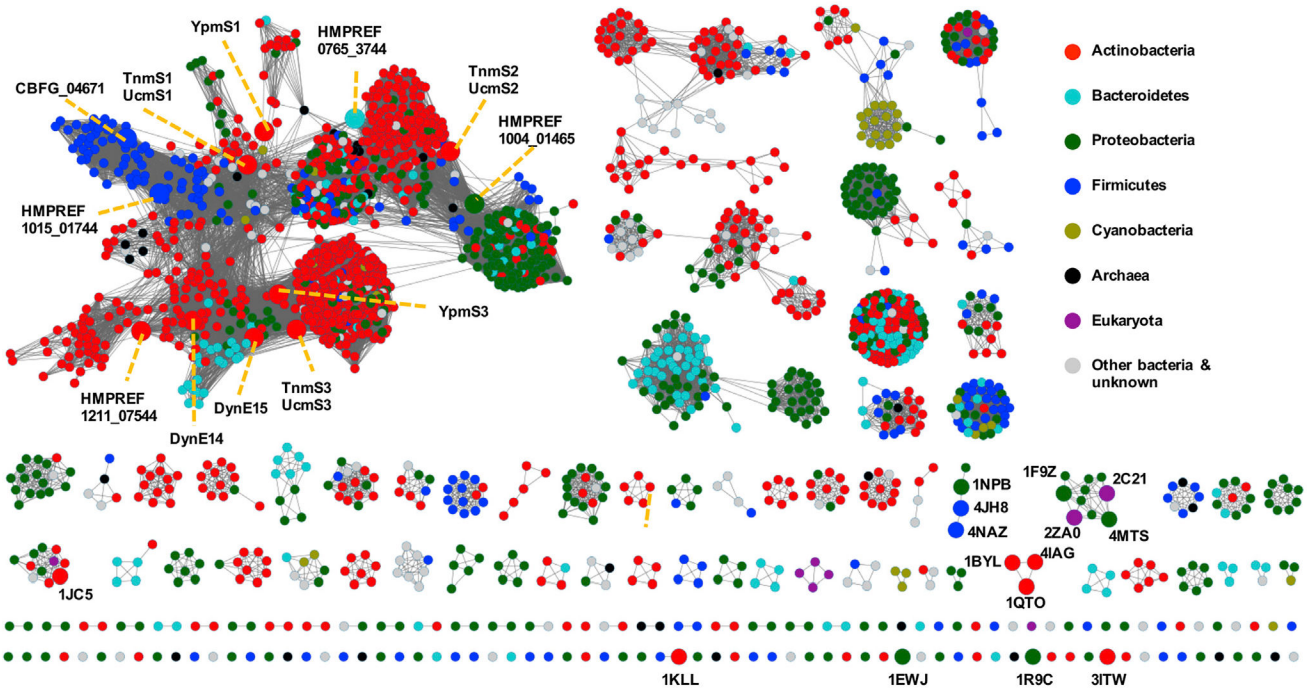

Figure 5. Sequence Similarity Network of Proteins from the InterPro Family IPR029068 Revealing Homologs of TnmS1, TnmS2, and TnmS3 Are Widely Distributed in Nature, Including the Human Microbiome

The SSN of the IPR029068 family was generated using the online Enzyme Function Initiative-Enzyme Similarity Tool (Gerlt et al., 2015) and visualized with Cytoscape with an *e* value threshold of 10^{-20} (~30% sequence identity over 80 amino acids). Each node represents proteins with above 75% sequence identities. The nodes are colored by the taxonomy of the sources of these proteins. The TnmS1, TnmS2, TnmS3, and their homologs characterized in this study are highlighted in larger circles and labeled with orange dashed lines. Other characterized proteins from the IPR029068 family are also highlighted in large circles and labeled with their respective PDB numbers. PDB: 1NPB, 4JH8, and 4NAZ are thiol transferases; PDB: 1F9Z, 2C21, 2ZA0, and 4MTS are glyoxalases-I; PDB: 1BYL, 4IAG, 1QTO, and 1EWJ are BLM binding proteins; PDB: 1JC5 is epimerase; PDB: 1KLL is mitomycin binding protein; PDB: 1R9C is epoxide hydrolase; and PDB: 3ITW is thiocoraline binding protein.

Table 1.

Sensitivity of Selected Streptomyces and *E. coli* Strains against TNM A as Determined by the MICs Values

Strain	MIC (ng/mL)
Streptomyces strains	
CB03234	500
SB20003	4
S. *lividans* TK24	4
E. coli strains	
BL21(DE3)/pET28a	2.5
SB20004 (TnmS1)	2,560
SB20005 (TnmS2)	2,560
SB20006 (TnmS3)	20,480
SB20014 (HMPREF1015_01744)	40
SB20015 (HMPREF0765_3744)	40
SB20016 (HMPREF1004_01465)	10
SB20017 (HMPREF1211_07544)	20,480
SB20018 (CBFG_04671)	1,280

Table 2.

Binding of TnmS1, TnmS2, TnmS3 and the Selected Homologs from the Human Microbiome to TNM A, TNM C, and Riboflavin as Determined by the K_D Values

Protein	Ligand	K_D (nM)
TnmS1	TNM A	163 ± 17
	TNMC	350 ± 41
	riboflavin	(84.1 ± 13.5) × 10^3
TnmS2	TNM A	246 ± 36
	TNM C	361 ± 65
	riboflavin	(59.5 ± 8.6) × 10^3
TnmS3	TNM A	108 ± 13
	TNM C	215 ± 27
	riboflavin	(1.1 ± 0.1) × 10^3
HMPREF1211_07544	TNM A	164 ± 23
CBFG_04671	TNM A	855 ± 66